23. Tam, P. P. & Behringer, R. R. Mouse gastrulation: the formation of a mammalian body plan. *Mech. Dev.* **68,** 3–25 (1997).
24. Wilson, V., Manson, L., Skarnes, W. C. & Beddington, R. S. The T gene is necessary for normal mesodermal morphogenetic cell movements during gastrulation. *Development* **121,** 877–886 (1995).
25. Wilson, V., Rashbass, P. & Beddington, R. S. Chimeric analysis of T (Brachyury) gene function. *Development* **117,** 1321–1331 (1993).
26. Ciruna, B. G., Schwartz, L., Harpal, K., Yamaguchi, T. P. & Rossant, J. Chimeric analysis of fibroblast growth factor receptor-1 (Fgfr1) function: a role for FGFR1 in morphogenetic movement through the primitive streak. *Development* **124,** 2829–2841 (1997).
27. Sun, X., Meyers, E. N., Lewandoski, M. & Martin, G. R. Targeted disruption of Fgf8 causes failure of cell migration in the gastrulating mouse embryo. *Genes Dev.* **13,** 1834–1846 (1999).
28. Wattler, S., Russ, A., Evans, M. & Nehls, M. A combined analysis of genomic and primary protein structure defines the phylogenetic relationship of new members of the T-box family. *Genomics* **48,** 24–33 (1998).
29. Hogan, B., Beddington, R., Constantini, F. & Lacy, E. *Manipulating the Mouse Embryo* (Cold Spring Harbor Laboratory Press, New York, 1994).

Acknowledgements

We thank J. Gurdon, A. Bulfone, A. Zorn, N. Papalopulu, D. St. Johnston and R. Pedersen for discussion; X. Sun and F. Beck for communicating results before publication; G. Martin, C. Wright and R. Milner for gifts of probes and reagents; F. Wianny and A. Sossick for help with confocal microscopy; J. Wilson for technical assistance; J. Ferguson, P. Whiting and R. Plumridge for animal care. A.P.R. thanks W. Gross for continuing support and advice. This work was funded by grants from the Wellcome Trust. V.W. is supported by a Medical Research Council Career Development Award.

Correspondence and request for materials should be addressed to A.P.R. (e-mail: apr@mole.bio.cam.ac.uk).

p73-deficient mice have neurological, pheromonal and inflammatory defects but lack spontaneous tumours

Annie Yang*, Nancy Walker†, Roderick Bronson‡, Mourad Kaghad†, Mariette Oosterwegel§, Jacques Bonnin†, Christine Vagner†, Helene Bonnet†, Pieter Dikkes‖, Arlene Sharpe§, Frank McKeon* & Daniel Caput†

* *Department of Cell Biology, Harvard Medical School, Boston, Massachusetts 02115, USA*
† *Sanofi Recherche, Innopole B.P. 137, 31676 Labege Cedex, France*
‡ *U.S. Department of Agriculture, Human Nutrition Research Center on Aging, and Department of Pathology, Tufts University of School of Veterinary Medicine, Boston, Massachusetts 02111, USA*
§ *Immunology Research Division, Departments of Pathology, Brigham and Women's Hospital and Harvard Medical School, Boston, Massachusetts 02115, USA*
‖ *Department of Neurology, Division of Neuroscience, Children's Hospital, Boston, Massachusetts 02115, USA*

p73 (ref. 1) has high homology with the tumour suppressor p53 (refs 2–4), as well as with *p63*, a gene implicated in the maintenance of epithelial stem cells[5–7]. Despite the localization of the p73 gene to chromosome 1p36.3, a region of frequent aberration in a wide range of human cancers[1], and the ability of p73 to transactivate p53 target genes[1], it is unclear whether p73 functions as a tumour suppressor. Here we show that mice functionally deficient for all p73 isoforms exhibit profound defects, including hippocampal dysgenesis, hydrocephalus, chronic infections and inflammation, as well as abnormalities in pheromone sensory pathways. In contrast to p53-deficient mice, however, those lacking p73 show no increased susceptibility to spontaneous tumorigenesis. We report the mechanistic basis of the hippocampal dysgenesis and the loss of pheromone responses, and show that new, potentially dominant-negative, p73 variants are the predominant expression products of this gene in developing and adult tissues. Our data suggest that there is a marked divergence in the physiological functions of the p53 family members, and reveal unique roles for p73 in neurogenesis, sensory pathways and homeostatic control.

Our analysis of murine *p73* complementary DNAs revealed transcripts encoding p73 proteins that lack an amino-terminal transactivation domain (ΔN-p73), in addition to those that show the carboxy-terminal diversity reported for human p73 (Fig. 1a)[1,8]. Like the transcripts encoding ΔN-p63 (ref. 5), the ΔN-p73 messages are derived from an alternative promoter located in intron 3. ΔN-p73 failed to activate transcription from a p53-reporter gene (data not shown) but suppressed the transactivation activity of p73α by hetero-oligomerization and competition for DNA binding (Fig. 1b, c). *In situ* hybridization experiments on mouse embryos failed to detect p73β, γ or δ transcripts, whereas p73α messenger RNA was highly expressed in a number of epithelial and neural structures, including nasal epithelium, the vomeronasal organ, the hippocampus and the hypothalamus (Fig. 1d; and data not shown). Additional probes revealed that ΔN-p73 transcripts appeared to be the predominant p73 gene product in adults (data not shown) and during embryogenesis (Fig. 1e).

Mice with disrupted *p73* alleles were produced using homologous recombination in embryonic stem (ES) cells to replace exons 5 and 6, which encode the DNA-binding domain, with the neomycin-resistance (NEO^R) gene[9,10] (Fig. 1f). The offspring of *p73* heterozygous mice showed a mendelian distribution of genotypes indicating that p73, like p53, is not required for embryogenesis[11,12] (Fig. 1g). Polymerase chain reaction with reverse transcriptase (RT-PCR) and sequence analysis of RNA from murine embryonic fibroblasts (MEFs) of known p73 genotypes confirmed the disruption of the *p73* gene (Fig. 1g).

$p73^{-/-}$ pups showed a runting phenotype and high rates of mortality (Fig. 2a, b). Most commonly, death followed massive gastrointestinal haemorrhages, although intracranial bleeding was apparent in ~15% of the mortalities. Histological examinations of the gastrointestinal tract of the $p73^{-/-}$ postnatal day 7 (P7) mice revealed numerous abnormalities including erosion marked by a loss of enterocytes and excessive mucosecretions in the duodenum, ileum and cecum (Fig. 2c; and data not shown), which may underlie the wasting syndrome and the intestinal haemorrhaging in these mice.

A striking feature of the $p73^{-/-}$ mice was severe rhinitis and purulent otitis media (Fig. 2d; and data not shown). Massive neutrophil infiltrates of these sites were obvious at the earliest ages examined (P2 pups) and persisted through adulthood, when greater than 80% of $p73^{-/-}$ mice exhibited chronic, bilateral rhinitis, otitis, periorbital oedema and conjunctivitis. Microbiological analysis of affected sites from $p73^{-/-}$ weanlings (P21) revealed the presence of *Escherichia coli*, *Pasteurella aerogenes* and micrococcal species. Despite these indications of inflammation and infection, no obvious deficiencies in lymphoid or granulocyte populations were detected in the $p73^{-/-}$ mice, indicating that there might be defects in other components of the natural immune system. In support of this notion, *p73* was highly expressed in the epithelia bordering the sites of infections in P21 mice (Fig. 2e). These epithelia function, in part, as barriers to external pathogens through secretion of mucus, cytokines and antimicrobial factors[13]. Despite the massive sinus inflammation marked by mucoserous secretions, neutrophil infiltration and goblet cell hyperplasia of the surrounding epithelia in the P2 pups (data not shown), these pups also lacked obvious Gram-staining pathogens. Together, these data indicate that the infections seen in the older pups may be, as with cystic fibrosis[14,15], the result of inappropriate or hyperactive epithelial responses, which in turn render these sinuses habitable by microorganisms. These observations raise the possibilities that the infections in the $p73^{-/-}$ mice are secondary to constitutive inflammatory signals promoted by the loss of p73, and may be linked to the gastrointestinal phenotype as a generalized pan-mucositis.

The $p73^{-/-}$ mice also show a mild, congenital hydrocephalus that progresses in some animals to a highly morbid condition marked by massive expansion of the lateral ventricles, compression of the cortex and intraventricular bleeding (Fig. 2f). Our analysis revealed a communicating form of hydrocephalus in these mice, indicating that there might be defects in production or reabsorption of cerebral spinal fluid (CSF)[16]. Precedence for the overproduction of CSF leading to hydrocephalus is found in mice lacking the transcription factor, E2F-5; these mice also develop a nonobstructive hydrocephalus[17]. Moreover, just as E2F-5 is abundant in the choroid plexus[17], p73 is highly expressed in the epithelial cells of the choroid plexus and in the ependymal cells lining the ventricles (not shown), both of which regulate CSF secretion and reabsorption. These data show that p73 is critical in regulating the homeostasis of CSF dynamics and raise the possibility of p73 interactions with E2F-5 in these processes.

Examination of the brains of the $p73^{-/-}$ mice revealed hippocampal dysgenesis, which is characterized by unusual arrangements of the CA1–CA3 pyramidal cell layer and the dentate gyrus (Fig. 3a, b). The dentate gyrus lacked an infrapyramidal blade and the suprapyramidal blade appeared hypertrophied and extended (Fig. 3a, b), which overall suggest an organization defect rather than a deficit of granular neurons. No major structural abnormalities were observed in other areas of the $p73^{-/-}$ brain, including the neocortex and cerebellum. Although defects in neurogenesis have been described

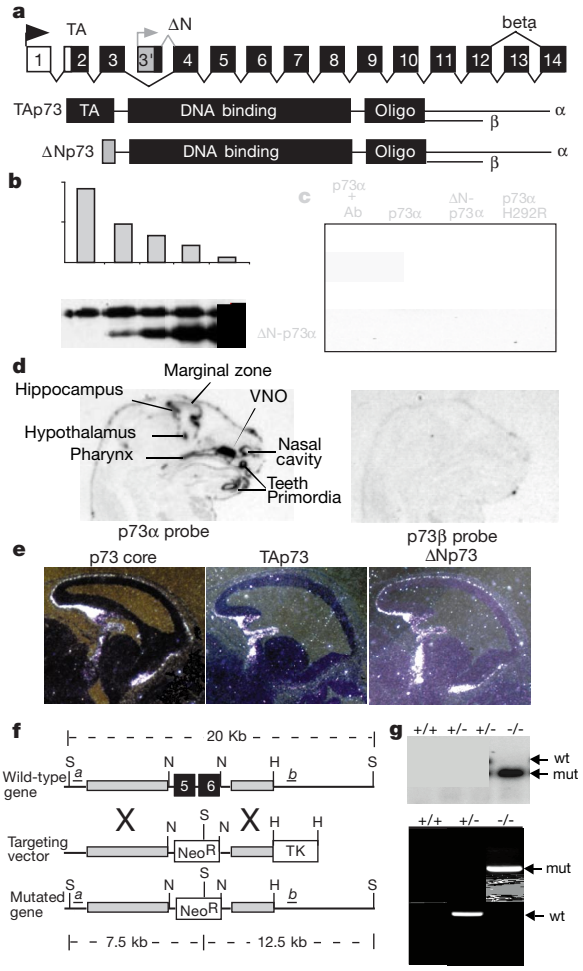

Figure 1 Targeted disruption of the murine *p73* gene. **a**, Murine *p73* structure depicting the transcriptional start positions of the two major promoters and the alternative splicing events that, together, give rise to the p73α, p73β, ΔNp73α and ΔNp73β transcripts. **b**, Transactivation and suppression analysis of p73 isotypes expressed in mammalian cells. Upper panel, luciferase activity after co-transfection of a luciferase p53-reporter construct and p73α with increasing ratio of ΔNp73α expression vector. Lower panel, anti-p73 western blot of cellular extracts analysed in the transcription assays. **c**, Gel-shift analysis of radiolabelled oligonucleotide containing p53 sites following incubation with *in vitro* translated p73α, ΔNp73α or mutant (H292R) p73α. Supershifting (lane1) was done with anti-p73 antibodies. **d**, *In situ* hybridization of sagittal sections of E18 mouse embryo with antisense probes corresponding to the p73α C terminus (left panel), and the p73β C terminus (right). VNO, vomeronasal organ. **e**, *In situ* hybridization analysis of sagittal sections through the telencephalon of an E12.5 embryo using p73 DNA binding (left), transactivation (middle) and ΔN (right) probes. **f**, Targeting strategy for disruption of murine *p73* gene. Approximate sizes of hybridizing fragments are indicated. H, *Hin*dIII; N, *Nhe*1; S, *Spe*1, kb, kilobases. **g**, Top, Southern blot analysis of tail DNA from offspring of matings between $p73^{+/-}$ mice. Wildtype (wt) and mutant (mut) alleles are indicated. Bottom, RT-PCR analysis of RNA from fibroblasts of embryos with indicated *p73* genotypes.

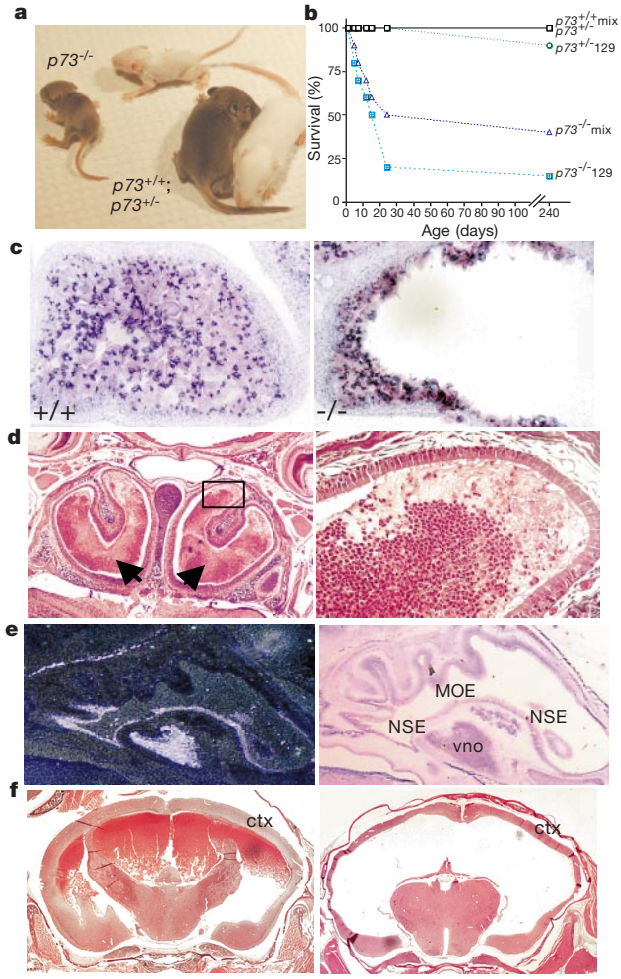

Figure 2 Somatic growth defects and mortality in $p73^{-/-}$ pups. **a**, Size comparison of 10-day-old pups with indicated *p73* genotypes. **b**, Mortality curves of $p73^{-/-}$, $p73^{+/-}$ and $p73^{+/+}$ mice of SJ129 or mixed backgrounds. **c**, Comparison of gastrointestinal tract of wild-type and $p73^{-/-}$ P7 mice. Histological sections of wild-type (left panel) and mutant ileum (right panel) revealing distended and eroded appearance of the mutant ileum. **d**, Left, transverse section at level of nasal passages of pre-weaning $p73^{-/-}$ mouse revealing purulent rhinitis (arrows). Right, higher magnification image of boxed region showing neutrophils and mucosecretions. **e**, Left, *in situ* hybridization of sections of wild-type P21 pups using probe to p73. Right, corresponding toluidine blue-stained section. NSE, nasal sinus epithelium; VNO, vomeronasal organ; MOE, main olfactor epithelium. **f**, Histological sections through skulls of P21 $p73^{-/-}$ mice displaying domed crania revealing expansion of ventricles, compression of the cortex (ctx) and intracranial haemorrhaging.

in several mouse models, particularly the *reeler* and *scrambler* mutants, these phenotypes reflect a generalized defect in neuronal migration affecting lamination in the cortex, hippocampus and cerebellum[18,19], and are therefore distinct from the dysgenesis observed in the $p73^{-/-}$ mice. It was thus interesting that in mid-gestation embryos p73 expression closely mirrored the expression patterns of reelin, a secreted glycoprotein which is essential for neuronal migration in the cortex[20–24]. In E12.5 animals, for example, cells lining the outer preplate layer of the telencephalic vesicles, the bed nucleus of the stria terminalis and the preoptic area (Fig. 3c) all stain positively for both reelin and p73. The correlation between p73 and reelin diverged in the wild-type, postnatal (P3) brain, where the two proteins were found to be co-expressed only in a distinct population of large, bipolar cells, known as the Cajal–Retzius neurons (CR), distributed in a continuous band along the marginal zone of the cortex extending to the molecular layer of the dentate gyrus (Fig. 3d, e). Other sites of reelin expression, including the cerebellum, cortical layer five and the olfactory bulb, were devoid of p73 signal (Fig. 4a). Notably, the $p73^{-/-}$ P3 brain showed an absence of reelin expression specifically in the marginal zone and the molecular layer of the dentate gyrus (Fig. 4b, c), whereas reelin expression in the cerebellum, cortical layer five and the olfactory bulb was similar to that of wild-type mice. In addition to the lack of reelin, we also failed to detect a second CR marker, calretinin, in the cortical and hippocampal marginal zones (data not shown).

These data indicate that functional loss of p73 leads to the disappearance of the CR neurons in the cortical marginal zone and hippocampal molecular layer, and that this defect underlies the hippocampal dysgenesis seen in p73-deficient mice. Notably, the loss of CR neurons in the $p73^{-/-}$ mouse is not accompanied by a cortical lamination defect, as seen in the reeler mouse. Moreover, the hippocampal dysgenesis of $p73^{-/-}$ mice is clearly distinct from the hippocampal defect of the reeler mouse[18]. Together, these findings indicate that p73-dependent CR neurons produce factors other than reelin to effect hippocampal neurogenesis. The link between the absence of these CR neurons and the striking yet highly site-specific dysgenesis in the $p73^{-/-}$ brain further suggests that CR

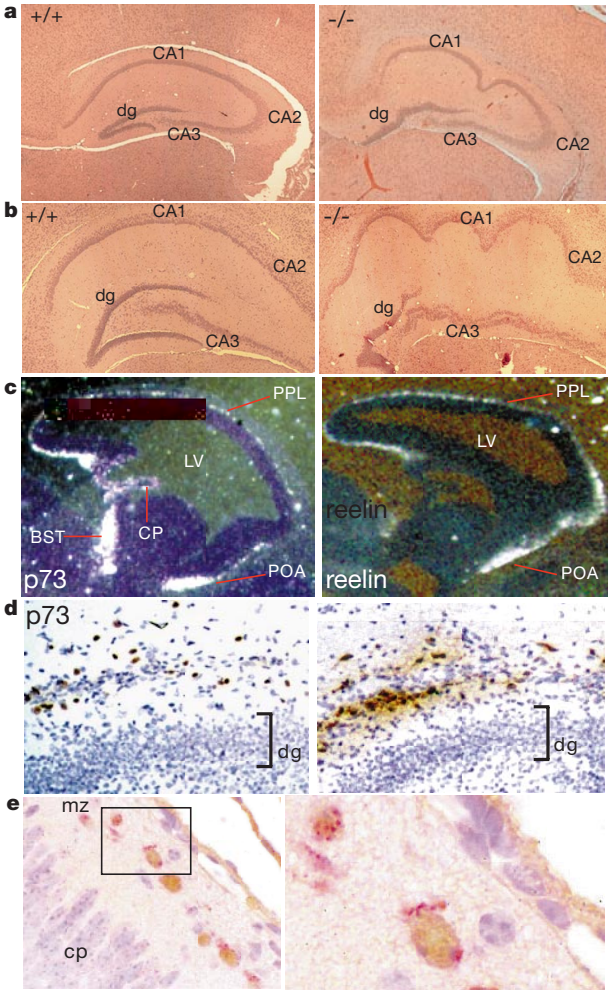

Figure 3 Hippocampal dysgenesis and reelin expression. **a**, Comparisons of hippocampal formation of rostral portions of wild-type and $p73^{-/-}$ mice. **b**, Comparison of hippocampal formation in caudal portions of the brains of wild-type and mutant mice. **c**, Left, *in situ* hybridization of p73 probe on E12.5 wild-type brain showing labelling of preplate layer (PPL) of the telencephalic vesicle, choroid plexus (CP), bed nucleus of the stria terminalis (BST), and preoptic area (POA). Right, E12.5 brain section following *in situ* hybridization of a reelin probe, revealing a similar pattern to that seen with the p73 probe with the exception of the choroid plexus. **d**, Left, p73 immunohistochemistry on sections of wild-type hippocampus revealing cells with nuclear staining (brown) in the molecular layer of the dentate gyrus. dg, dentate gyrus granule cells. Right, Reelin immunohistochemistry on sections of wild-type hippocampus revealing positive cells surrounded by matrix of secreted reelin (brown) in the molecular layer of the dentate gyrus. **e**, Left, co-localization of immunohistochemical staining of p73 (brown) and reelin (red) in cells of the marginal zone of the cerebral cortex. Right, higher magnification.

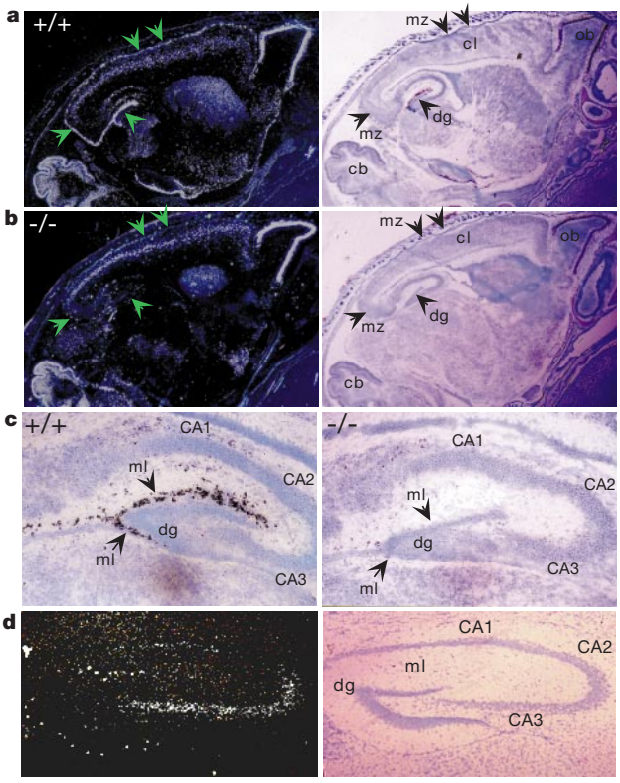

Figure 4 Reelin expression in wild-type and $p73^{-/-}$ P3 mice. **a**, Left, *in situ* hybridization of reelin probe on P3 wild-type brain. Right, corresponding stained section. mz, marginal zone; dg, dentate gryus; cl, cortical layer; ob, olfactory bulb; cb, cerebellum. **b**, Left, *in situ* hybridization of reelin probe on P3 *p73* mutant brain. Right, corresponding stained sections. Green arrows mark regions of loss of reelin-positive cells in the $p73^{-/-}$ brain. **c**, Left, *in situ* hybridization (black granules) of reelin in the wild-type hippocampus. Right, corresponding image in the mutant hippocampus, revealing loss of reelin expression in molecular layer (ml, arrows) of the dentate gyrus (dg). CA1, CA2 and CA3, subregions of pyramidal cell layer. **d**, Left, p73 *in situ* hybridization of P21 wild-type hippocampus showing signal at CA3 and CA1 pyramidal neurons and cells in the molecular layer (ml) of the dentate gyrus (dg). Right, corresponding toluidine blue stained section.

cells, widely believed to control cortical neurogenesis, may instead have a critical role in hippocampal development. Finally, p73 expression is maintained in P21 CR neurons of the hippocampal molecular layer (Fig. 4d), indicating that p73 may function in the modelling of persistent neurogenesis of the dentate gyrus throughout adulthood[25,26].

The p73-deficient male mice lacked both interest in sexually mature females and aggressive responses to other males. To quantify this defect, 15 $p73^{-/-}$ males, age 6–10 weeks, were housed with three wild-type females each and pregnancies scored after 30 days. Only one pregnancy was obtained from these matings, whereas most females (>90%) housed with wild-type males were pregnant by 30 days. Likewise, no pregnancies were observed in female $p73^{-/-}$ mice that mated with wild-type males, indicating a defect in conceiving or maintaining embryos. No structural abnormalities in the reproductive organs of either male or female $p73^{-/-}$ mice were observed by histology, suggesting, instead, that they might have defects in hormonal or sensory pathways[27,28]. The highest levels of p73 RNA in the mouse were found in the neuroepithelium of both the embryonic and adult vomeronasal organ (VNO), an accessory olfactory structure involved in pheromone detection (Fig. 5a). Given this, and the behavioural and reproductive abnormalities in $p73^{-/-}$ mice, p73 deficiency might affect VNO function. We examined the expression patterns of the two structurally distinct classes of pheromone receptors present in the VNO, V1R and V2R[29,30]. The wild-type VNO showed numerous V2R- and V1R-expressing cells, but no cells were positive in the $p73^{-/-}$ VNO (Fig. 5b). Similarly, expression of olfactory cell adhesion molecule (OCAM), a marker of neurosensory cells of the main olfactory epithelium (MOE) and the VNO, was absent from the VNO of $p73^{-/-}$ mice (Fig. 5c). OCAM expression was normal in the MOE of the $p73^{-/-}$ mouse (data not shown), suggesting a site-specific consequence of p73 loss on these related cell populations. The lack of OCAM and V1R and V2R recetors was not attributable to a gross absence of cells in the VNO, as probes for the olfactory marker protein (OMP), expressed by differentiated chemosensory neurons of the VNO and MOE, revealed strong expression in both wild-type and mutant VNOs (Fig. 5d). Finally, the p73 signal was also intense in secondary and tertiary projections of the accessory olfactory system, including the accessory olfactory bulb, the amygdala and hypothalamus (data not shown), suggesting that additional defects in sensory or hormonal pathways may contribute to the reproductive and behavioural phenotypes of p73-deficient mice.

During this work, we carried out necropsies on over 100 $p73^{-/-}$ mice ranging in ages from 2 to 15 months, and found no increased tendency in these mice to develop spontaneous tumours. These data appear to preclude the notion that p73 functions in a manner similar to p53 to suppress tumour development; however, whether ΔN-p73 variants, which potentially counteract p53, modulate p53 activity in the cell remains unresolved.

Our data reveal a marked divergence in the respective developmental activities of *p63* and *p73* and further distinguish these genes from *p53*, the most recently evolved member of the family apparently devoted to tumour suppression. Despite these revelations, we know relatively little about specific gene targets for any member of the p53 family of transcriptional activators, or about the *in vivo* consequences of the predominant p63 and p73 isotypes, which lack transactivation domains and appear to have dominant-negative properties. The apparent requirement for p73 in such processes as pheromone detection, neurogenesis and fluid dynamics underscores the role of p73 in mechanisms of sensing environmental and homeostatic stimuli that may in turn represent paradigms adopted by p53 for sensing DNA damage and other cellular stresses. □

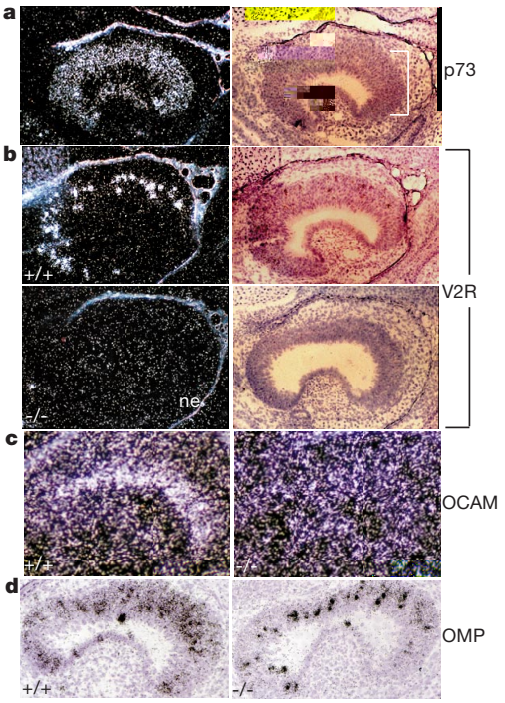

Figure 5 p73 and pheromone receptor expression. **a**, Left, autoradiograph of wild-type vomeronasal organ showing p73 transcript expression in the neurosensory epithelim (ne). Right, corresponding stained image showing structure of the vomeronasal organ. **b**, Left, autoradiograph of vomeronasal organ of wild-type (+/+; top) and mutant (–/–; bottom) mice hybridized with antisense probe to detect V2R family of pheromone receptors. Right, corresponding bright field images. **c**, Autoradiograph of wild-type (+/+) and mutant (–/–) VNO probed with olfactory cell adhesion molecule (OCAM) antisense oligonucleotide. **d**, Autoradiograph of wild-type (+/+) and mutant (–/–) VNO probed with an olfactory maturation protein (OMP) antisense oligonucleotide.

Methods

Targeted disruption of *p73* gene in embryonic stem cells

A 16.5 kb phage clone containing the 3′ end of intron 4 to exon 10 was isolated from a Lambda DASH-II 129/SvJae genomic library and subcloned into pZero vector (Invitrogen). To generate the targeting vector, a 1.4 kb *Nhe*I–*Nhe*I fragment, corresponding to exon 5, a portion of exon 6 and adjacent intronic sequences, was deleted and replaced with the neomycin drug-resistance (NEO^R) gene driven by the mouse phosphoglycerol kinase (PGK1) promoter and linked to the PKG1 poly(A) sequences. The targeting vector contained ~5.5 kb and 2.5 kb of homology upstream and downstream, respectively, of the $PGK–Neo^R$ gene and the *pMC-TK* gene[9] at its most 5′ end. The vector was linearized using a unique *Not*I site and electroporated into the JI ES cell line[10]. G418 and FIAU-resistant ES cell colonies were picked and expanded. Two distinct ES cell lines heterozygous for the disrupted allele were microinjected into blastocysts from B57BL/6 and BALB/c mice, and gave rise to germline transmission of the p73 mutation.

In situ hybridization

Frozen sections were post-fixed for 45 min in 4% paraformaldehyde at 4 °C, washed twice for 5 min in PBS at 4 °C, washed once for 5 min in PBS at room temperature, and dehydrated in 95% ethanol for 1 min. Oligonucleotides were 3′-end labelled with ^{35}S-dATP (Amersham) by terminal transferase (Promega). Radiolabelled probes were added to hybridization solution (10% dextran sulphate, 50% formamide, 1 × Denhardt's, 4 × SSC, 200 mM dithiothreitol (DTT). 250 μg ml poly(A)) and incubated overnight at 42 °C. Stringency washes were conducted by shaking the slides at 55 °C with 1 × SSC, 0.05% sarkosyl (SK), and 10 mM DTT. For the specific oligonucleotides, see Supplementary Information.

DNA transfection and luciferase assays

SK-NA-S (human neuroblastoma) cells were transfected with p53–luciferase reporter and p73 expression plasmids using Lipofectamine (Life Technologies). In a typical experiment, 1 μg of reporter plasmid p53RGC-Luc was co-transfected with 70 ng of pcDNA3 containing p73α cDNA and 70, 350 or 700 ng of pcDNA3 containing ΔN-p73α cDNA. The final DNA concentration was adjusted to 1.77 μg per well using pcDNA3. Twenty-four hours after transfection, luciferase activity was measured in cell lysates with the Dual Luciferase Reporter Assay System (Promega).

Gel-shift assays

p73α, p73α (R293H) or ΔN-p73α cDNA containing pcDNA-3 were transcribed and subsequently *in vitro* translated using TNT7-coupled reticulocyte lysate system (Promega). Each DNA-binding reaction contained 2.5 μl of reticulocyte lysate, 2.5 mM of DDT, 10 ng of ^{32}P-labelled DNA, 1 μg of salmon DNA as non-specific competitor, 12. μl of glycerol and Tris-buffered saline (TBS; 25 mM Tris pH 7.5, 130 mM NaCl, 3 mM KCl) to 10 μl final volume. Reactions were incubated at 23 °C for 30 min, cooled to 4 °C and electrophoresed in 4% non-denaturing polyacrylamide gel in a low salt buffer (0.4 × TBE).

Received 14 October 1999; accepted 19 January 2000.

1. Kaghad, M. *et al.* Monoallelically expressed gene related to p53 at 1p36, a region frequently deleted in neuroblastoma and other human cancers. *Cell* **90,** 809–819 (1997).
2. Kinzler, K. W. & Vogelstein, B. Life (and death) in a malignant tumour. *Nature* **379,** 19–20 (1996).
3. Ko, L. J. & Prives, C. p53: puzzle and paradigm. *Genes Dev.* **10,** 1054–1072 (1996).
4. Levine, A. J. p53, the cellular gatekeeper for growth and division. *Cell* **88,** 323–331 (1997).
5. Yang, A. *et al.* p63, a p53 homolog at 3q27-29, encodes multiple products with transactivating, death-inducing, and dominant-negative activities. *Mol. Cell* **2,** 305–316 (1998).
6. Yang, A. *et al.* p63 is essential for regenerative proliferation in limb, craniofacial and epithelial development. *Nature* **398,** 714–718 (1999).
7. Mills, A. A. *et al.* p63 is a p53 homologue required for limb and epidermal morphogenesis. *Nature* **398,** 708–713 (1999).
8. De Laurenzi, V. *et al.* Two new p73 splice variants, gamma and delta, with different transcriptional activity. *J. Exp. Med.* **188,** 1763–1768 (1998).
9. Capecchi, M. R. Altering the genome by homologous recombination. *Science* **244,** 1288–1292 (1989).
10. Li, E., Bestor, T. H. & Jaenisch, R. Targeted mutation of the DNA methyltransferase gene results in embryonic lethality. *Cell* **69,** 915–926 (1992).
11. Donehower, L. A. Mice deficient for p53 are developmentally normal but susceptible to spontaneous tumours. *Nature* **356,** 215–221 (1992).
12. Jacks, T. *et al.* Tumor spectrum analysis in p53-mutant mice. *Curr. Biol.* **4**, 1–7 (1994).
13. Kim, K. C. *et al.* Airway goblet cell mucin: its structure and regulation of secretion. *Eur. Respir. J.* **10,** 2644–2649 (1997).
14. Matsui, H. *et al.* Evidence for periciliary liquid layer depletion, not abnormal ion composition, in the pathogenesis of cystic fibrosis airways disease. *Cell* **95,** 1005–1015 (1998).
15. Cressman, V. L., Hicks, E. M., Funkhouser, W. K., Backlund, D. C. & Koller, B. H. The relationship of chronic mucin secretion to airway disease in normal and CFTR-deficient mice. *Am. J. Respir. Cell. Mol. Biol.* **19,** 853–866 (1998).
16. Go, K. G. The normal and pathological physiology of brain water. *Adv. Tech. Stand. Neurosurg.* **23,** 47–142 (1997).
17. Lindeman, G. J. A specific, nonproliferative role for E2F-5 in choroid plexus function revealed by gene targeting. *Genes Dev.* **12,** 1092–1098 (1998).
18. Stanfield, B. B. & Cowan, W. M. The morphology of the hippocampus and dentate gyrus in normal and Reeler mice. *J. Comp. Neurol.* **185,** 393–422 (1979).
19. Rakic, P. & Caviness, V. S. Jr Cortical development: view from neurological mutants two decades later. *Neuron* **14,** 1101–1104 (1995).
20. Ogawa, M. *et al.* The reeler gene-associated antigen on Cajal–Retzius neurons is a crucial molecule for laminar organization of cortical neurons. *Neuron* **14,** 899–912 (1995).
21. D'Arcangelo, G. *et al.* A protein related to extracellular matrix proteins deleted in the mouse mutant reeler. *Nature* **374,** 719–723 (1995).
22. Frotscher, M. Cajal–Retzius cells, Reelin, and the formation of layers. *Curr. Opin. Neurobiol.* **8,** 570–575 (1998).
23. D'Arcangelo, G. & Curran, T. Reeler: new tales on an old mutant mouse. *BioEssays* **20,** 235–244 (1998).
24. Alcantara, S. *et al.* Regional and cellular patterns of reelin mRNA expression in the forebrain of the developing and adult mouse. *J. Neurosci.* **18,** 7779–7799 (1998).
25. McEwen, B. S. Stress and hippocampal plasticity. *Annu. Rev. Neurosci.* **22,** 105–122 (1999).
26. Gage, F. H., Kempermann, G., Palmer, T. D., Peterson, D. A., Ray, J. Multipotent progenitor cells in the adult dentate gyrus. *J. Neurobiol.* **36,** 249–266 (1998).
27. Bargmann, C. I. Olfactory receptors, vomeronasal receptors, and the organization of olfactory information. *Cell* **90,** 585–587 (1997).
28. Tirindelli, R. & Mucignat-Caretta, C., Ryba, N. J. Molecular aspects of pheromonal communication via the vomeronasal organ of mammals. *Trends Neurosci.* **21,** 482–486 (1998).
29. Matsunami, H. & Buck, L. A multigene family encoding a diverse array of putative pheromone receptors in mammals. *Cell* **90,** 775–784 (1997).
30. Herrada, G. & Dulac, C. A novel family of putative pheromone receptors in mammals with a topographically organized and sexually dimorphic distribution. *Cell* **90,** 763–773 (1997).

Supplementary information is available on *Nature*'s World-Wide Web site (http://www.nature.com) or as paper copy from the London editorial office of *Nature*.

Acknowledgements

We would like to thank F. Borriello, H. Green, C. Westphal, P. Ferrara, T. Rapoport and L. Buck for helpful discussions; L. Du for blastocyst injections; A. Goffinet for the reelin antibody; H. Liu for the mouse genomic library; and J. Williams for histology preparation. This work was supported by the American Cancer Society and the Council for Tobacco Research (F.M.), and the NIH (R.B., A.S., P.D. and F.M.).

Correspondence and requests for materials should be addressed to F.M. (e-mail: fmckeon@hms.harvard.edu) or D.C. (e-mail: daniel.caput@wanadoo.fr).
GenBank accession codes for *M. musculus* p73α and *M. musculus* ΔN-p73α mRNAs are Y19234 and Y19235, respectively.

Single-molecule studies of the effect of template tension on T7 DNA polymerase activity

Gijs J.L. Wuite*, Steven B. Smith*, Mark Young†, David Keller‡ & Carlos Bustamante*

** Department of Physics and Department of Molecular and Cell Biology, University of California, Berkeley, California 94720, USA*
† Institute of Molecular Biology, University of Oregon, Eugene, Oregon 97403, USA
‡ Department of Chemistry, University of New Mexico, Albuquerque, New Mexico 87131, USA

T7 DNA polymerase[1,2] catalyses DNA replication *in vitro* at rates of more than 100 bases per second and has a 3′→5′ exonuclease (nucleotide removing) activity at a separate active site. This enzyme possesses a 'right hand' shape which is common to most polymerases with fingers, palm and thumb domains[3,4]. The rate-limiting step for replication is thought to involve a conformational change between an 'open fingers' state in which the active site samples nucleotides, and a 'closed' state in which nucleotide incorporation occurs[3,5]. DNA polymerase must function as a molecular motor converting chemical energy into mechanical force as it moves over the template. Here we show, using a single-molecule assay based on the differential elasticity of single-stranded and double-stranded DNA, that mechanical force is generated during the rate-limiting step and that the motor can work against a maximum template tension of

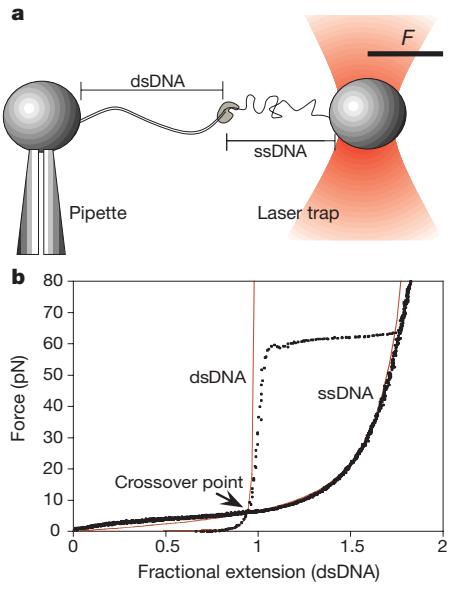

Figure 1 Optical trap setup. **a**, A 10,416-base pair plasmid DNA fragment was prepared as described[18] and attached between two beads, one held on the tip of a glass pipette, the other in an optical trap. Single-stranded DNA was obtained by using the force-induced exonuclease activity of T7 DNAp to remove any desired length of the non-template strand. The end-to-end length of the DNA was obtained by video imaging of the bead positions, and the force (F) was measured using the change in light momentum which exits the dual-beam trap[6]. **b**, Force–extension data for dsDNA and ssDNA (dotted lines), compared with the wormlike chain model using ssDNA and dsDNA persistence lengths of 0.7 nm and 53 nm respectively (solid lines)[7,8]. Difference between ssDNA and WLC curves at low tension is due to partial hairpin formation and disappears if magnesium is removed from buffer.